JMEPEG
https://doi.org/10.1007/s11665-020-04771-4

1059-9495/$19.00

High-Strength Low-Cost Nano-Bainitic Steel

Mohamad Akram, Heinz Palkowski, and Mohamed Soliman

(Submitted December 2, 2019; in revised form March 23, 2020)

Low-cost, fast-transforming carbide-free nano-bainitic steel has been produced with tensile strengths up to 2140 MPa and elongation values of around 10%. An alloying concept of combining low Mn (0.29 wt.%) and moderate Al (~ 1 wt.%) additions enabled full transformation in 10 min to less than 2 h at austempering temperatures ranging from 235 to 310 °C. Dilatometric experiments and thermodynamic simulation via ThermoCalc software were employed to design the heat treatment procedure. The resulting structures were investigated using scanning electron microscopy and synchrotron x-ray diffraction. Mechanical characterization was performed via hardness, tensile, and impact testing at room temperature. The strain-aging response for the alloy system was also investigated.

Keywords carbide-free bainite, low-temperature bainite, nano-bainite, phase transformation, retained austenite

1. Introduction

Carbide-free nano-bainitic steels offer an attractive mix of high strength and toughness coupled with inexpensive tailorability via low-temperature isothermal treatments (Ref 1-4). The key to generating the aforementioned steels is lowering the martensite start (Ms) temperature, suppressing carbide precipitation, and consequently generating an optimum microstructure of nano-sized bainitic ferrite platelets alternated with thin layers of retained austenite (Ref 5-8). While control over the phase amounts and sizes via low-temperature heat treatments presents a significant advantage over processing conventional high-strength steels, long transformation times and expensive alloying elements still hinder the full utilization of these alloys (Ref 1, 2, 9).

Certain alloying concepts are universal for the production of nano-bainite (nB). Silicon (Si)—around 2 wt.%—is added to inhibit cementite precipitation, which is a void nucleation phase detrimental to the impact properties of bainitic steels. The addition of Si, being insoluble in cementite, necessitates that it diffuses from the regions where cementite is to precipitate, a condition that is difficult to achieve under para-equilibrium conditions. The main idea behind accelerating the bainite transformation is increasing the stability difference between austenite and ferrite, hence encouraging the transformation former to the latter. Elements such as Co and Al increase the stability of ferrite with respect to austenite, thus accelerating the reaction, while Mn and C increase the stability of austenite, thus having the opposite effect (Ref 10).

Reported nB steels generally rely on extensive alloying to attain their intended structure (Ref 10, 11). Understanding the requirements for a successful nB production along with the roles of each element added is the key to a proper alloy design. The formation of nano-bainitic ferrite platelets requires austempering at low temperatures, necessitating an alloy with a low martensite start temperature, along with sufficient hardenability to avoid the formation of any undesirable ferrite and pearlite during cooling. However, the literature reports an optimum austempering value of 200 °C below which the properties of any nB generated are lowered (Ref 4, 12). An innate problem with nB formation is that the low temperatures used dictate slow kinetics and consequently long transformation times.

A continuous research effort is being made to reduce these transformation times via alloying additions and process modifications. Ausforming has been employed to accelerate the bainitic reaction. Deforming austenite prior to transformation increases the nucleation sites for bainite, reducing the incubation time and accelerating the transformation kinetics. However, it should be noted that there is a critical strain value beyond which the austenite strength becomes too high, so not plastically accommodating the formation of bainitic ferrite; hence, the transformation is adversely affected (Ref 5, 9, 13-15). Kabirmohammadi et al. managed to reduce the transformation time at 300 °C from 6 h down to 1 h for a 0.9% C, 1.0% Mn, 0.9% Al, and 1.8% Co alloy by ausforming to 25% thickness reduction (Ref 9). Hu et al. propose two opposing effects for ausforming, enhancing nucleation and retarding reaction kinetics. They suggest an optimum ausforming temperature of 350 °C above which the thickness of the bainite platelets increases for the ausformed condition compared to the non-ausformed ones (Ref 16). On the other hand, ausforming increases the percentage of retained austenite via mechanical stabilization, thus leading to a reduction in mechanical properties. In addition, the number of crystallographic variants in bainite decreases. This causes a reduction in the impact properties of the final microstructure, since the varying crystallographic orientations of bainitic sheaves force repeated changes in the crack path (Ref 5, 15). Hence, higher mechanical properties are expected from nB alloys that are accelerated via alloy design rather than ausforming.

Prior generation of a small fraction of martensite followed by austempering is expected to accelerate the bainitic transformation via the introduction of dislocations in the austenite grains, thus promoting the nucleation of bainitic ferrite (Ref 6, 17). In a study by Gong et al., the generation of 6% martensite

Mohamad Akram, Heinz Palkowski, and **Mohamed Soliman**, Institute of Metallurgy, Clausthal University of Technology, 38678 Clausthal-Zellerfeld, Germany. Contact e-mails: mohamad.abdelaziz@tu-clausthal.de, heinz.palkowski@tu-clausthal.de, and mohamed.soliman@tu-clausthal.de.

Published online: 16 April 2020

prior to austempering accelerated the rate of bainite transformation through the reduction in the incubation time, while the kinetics of the transformation remained unchanged. It was reported that the accelerating effect of martensite introduction was less significant than that of ausforming, as the dislocations introduced by the martensite are localized at the martensite-austenite boundaries, while ausforming produces a homogenous distribution of dislocations throughout the structure (Ref 6).

A technique used to stabilize austenite at lower carbon percentages is intercritical annealing, generating intercritical ferrite (ICF), which enriches the surrounding austenite by carbon diffusing out of it (Ref 7). This process has been reported to yield two contradicting effects on the bainite transformation kinetics: The generation of ICF reduces the maximum possible fraction of bainite formed, hence accelerating the transformation, while the austenite enrichment has the opposite effect (Ref 18). Soliman and Palkowski report that the presence of ICF in the vicinity of γ_r islands serves to stabilize the latter, consequently reducing the adverse effect that the γ_r islands have on the mechanical properties and improving the alloy's ductility. On the other hand, it has been reported that the introduction of ICF into the microstructure diminishes the tensile properties of the steel produced while improving the compressive strength and fracture strain (Ref 8, 18, 19).

A prerequisite to proper nB alloy design is the understanding of the effect of the common steel alloying additions on the bainitic transformation and final properties. The bainitic transformation kinetics is a function of the relative stabilities of the ferrite and austenite phases at the transformation temperature. On the other hand, the strength of an nB alloy is a function of the bainitic ferrite content and its lamellar thickness, while its ductility is governed by the amount and morphology (hence stability) of the retained austenite in the microstructure (Ref 20, 21). As previously mentioned, Mn is commonly added to improve the hardenability of nB steels. However, its addition retards the bainite formation kinetics, as well as shifts the T_0 curve toward lower carbon contents, resulting in a higher amount of retained austenite in the microstructure. Since the amount of retained austenite governs the ductility of nB alloys, it might be expected for the ductility of nB to increase with the Mn content; however, as the amount of retained austenite increases, the fraction of blocky unstable retained austenite also increases in the microstructure, which easily transforms to martensite upon cooling or at low levels of loading, jeopardizing the ductility of the alloy (Ref 21). Other common hardenability elements that could be used to replace Mn are Cr and Ni. Yang et al. attempted to substitute high carbon additions with high Ni additions and report a decrease in the difference between the bainite and martensite start temperatures as well as a tendency for the bainite lamellae to coalesce at high Ni contents. In addition to that, the transformation times resulting from this alloying strategy were reported to be too long to be considered for industrial application (Ref 22). While Cr is known as a ferrite stabilizer, it has a minimal effect on the free energy difference between austenite and ferrite and hence does not positively influence the bainitic transformation kinetics. Wang et al. report that Cr has a similar effect to Mn on the incubation period for bainitic transformation, prolonging it and thus slowing the overall transformation kinetics (Ref 23).

Caballero and Bhadeshia proposed that a reduction in Mn% would substantially accelerate the transformation kinetics. This idea, however, has not gained much traction in the literature (Ref 10). A patented medium-carbon steel alloy (0.55 wt.% C) designed by Ref 24 managed to reduce the transformation time at 300 °C to 48 min by dropping the Mn content to 0.37 wt.%, with 0.9 wt.% Al and 1.9 wt.% Co added to accelerate the transformation kinetics. A recent publication by Tiang et al. reports that while the addition of Al accelerates the transformation kinetics and improves the total elongation, it leads to a slight decrease in tensile strength (Ref 25).

While the current literature explores a variety of options for nB acceleration, very few offer a combination of low-cost alloying strategies, fast transformation time, and high mechanical properties. The objective of the current investigation is to develop an nB steel alloy that fills this gap. In this respect, expensive elements such as Co, Ni, and Cr are to be excluded to minimize the cost. Additionally, the addition of Al and the reduction of Mn were employed to accelerate the bainitic reaction.

2. Materials and Methods

Simple concepts were utilized in designing the investigated alloys: Mn was reduced to accelerate the transformation kinetics; on the other hand, the amount of Mn was not to fall below the minimum amount needed to prevent formation of iron sulfide. Mn actively reacts with iron sulfides during solidification forming ductile manganese sulfide. Si was added to inhibit cementite formation, its percentage lower than the usual 2 wt.% due to the presence of 0.9% Al, which serves the dual purpose of accelerating the bainite transformation and inhibiting cementite precipitation. Mo was added to improve hardenability and counter temper embrittlement.

ThermoCalc software was used to calculate the phase diagrams of the studied alloys to estimate their austenization temperatures. Dilatometric testing was performed using a BährDil 805A dilatometer on 5 × 10 mm cylindrical specimens machined from the rolled plates.

The alloys were cast in a vacuum furnace into blocks with dimensions 31 × 31 × 150 mm^3, homogenized for 48 h in argon atmosphere, followed by cooling for 12 h in argon atmosphere by switching off the oven. The homogenized blocks were hot rolled at 1100 °C to 8 mm thickness using a 12" two-high rolling machine followed by oven cooling in argon atmosphere. The compositions of the rolled plates are given in Table 1.

Vickers (HV20) hardness testing was performed according to ASTME92-83. Transformed dilatometry specimens were prepared by grinding down to 400 grid size before testing via a Wolpert hardness tester equipped with a digital measurement system. Dilatometry specimens were then tempered at 200 °C

Table 1 Chemical composition of the studied alloys in wt.%

Alloy	C	Mn	Si	Al	Mo	Fe
A11	0.54	0.29	1.41	0.92	0.55	Bal.
A12	0.67	0.29	1.39	0.95	0.55	Bal.
A13	0.80	0.29	1.35	0.97	0.56	Bal.

for 2 h to reveal any possible martensite during microscopy. Specimens were ground and polished using standard techniques followed by deep Nital etching, and gold sputtering for viewing under scanning electron microscope (SEM).

ASTM E8 sub-size round tensile specimens with a gauge length of 12.5 mm and diameter of 2.5 mm were machined from the hot-rolled plates along their rolling direction (Ref 26). Specimens intended for strain aging were subjected to a 2% pre-strain followed by isothermal holding at 170 °C for 20 min. Tensile testing was performed on a Zwick/Roell universal testing machine with a 250 kN load cell. The machine is equipped with a video extensometer for accurate strain measurements. A 10 MPa s^{-1} loading rate was used in the elastic region, changing into a loading speed of 0.0115 mm s^{-1} during the yielding stage and finally changing into 0.0067 s^{-1} in the plastic region. This loading plan is based on the DIN-68921 standard for bake hardening measurements (Ref 27). ASTM E23 sub-size notched Charpy impact specimens with dimensions of 5 × 5 × 50 mm^3 were machined in the rolling direction from the rolled steel plates (Ref 28). Austenitization and austempering temperatures used are listed in the following section. All mechanical testing specimens were isothermally transformed in the dilatometer.

Synchrotron XRD analysis was performed at the DeutschesElektronen-Synchrotron (DESY) facility in Hamburg, Germany, on transformed dilatometry specimens, and retained austenite percentages were calculated from the integrated intensities of the (111), (200), (220), and (311) austenite diffraction peaks and the (110), (200), (211), and (220) ferrite diffraction peaks according to the method described by Cullity (Ref 29).

3. Results

3.1 The As-Rolled Material

Figure 1 shows LOM images of the three alloys in the as-rolled condition. The structure of the alloys is composed of ferrite and pearlite. The ferrite content decreases gradually with increasing the carbon content. The observation of a fully pearlitic structure in A13 indicates the occurrence of the eutectoid point at this composition (0.80 wt.% C).

Figure 2(a) shows the phase diagram of the alloy group calculated using ThermoCalc software. As shown in this figure, the simulations predict the occurrence of the eutectoid point at 0.89 wt.% C, which is higher than the actually observed carbon content of the eutectoid point as indicated above. Figure 2(b) shows the comparison of the pro-eutectoid ferrite percentages obtained from the ThermoCalc simulation with the experimentally obtained values (i.e., values of the ferrite contents of alloys A11, A12, and A13), and it seems that the simulated values deviate from the experimentally ones at higher carbon contents.

3.2 Dilatometry

Thermodynamic simulation using ThermoCalc software indicates that the full austenitization temperatures (A_{e3}) are 860, 816, and 781 °C for A11, A12, and A13 alloys (Fig. 2a), respectively. Full austenitization is essential prior to austempering, and 50 °C above the A_{e3} temperature would be sufficient. However, the values obtained from the thermodynamic calculations for A_{e3} may deviate significantly from the actual values as previously reported (Ref 30). Accordingly, an austenitization temperature of 950 °C was chosen for all the alloys in this study to ensure full austenitization with a sufficient margin of safety to account for a deviation of up to 40 °C between the simulations and experimental results. Dilatometry specimens were heated at a rate of 10 K s^{-1} up

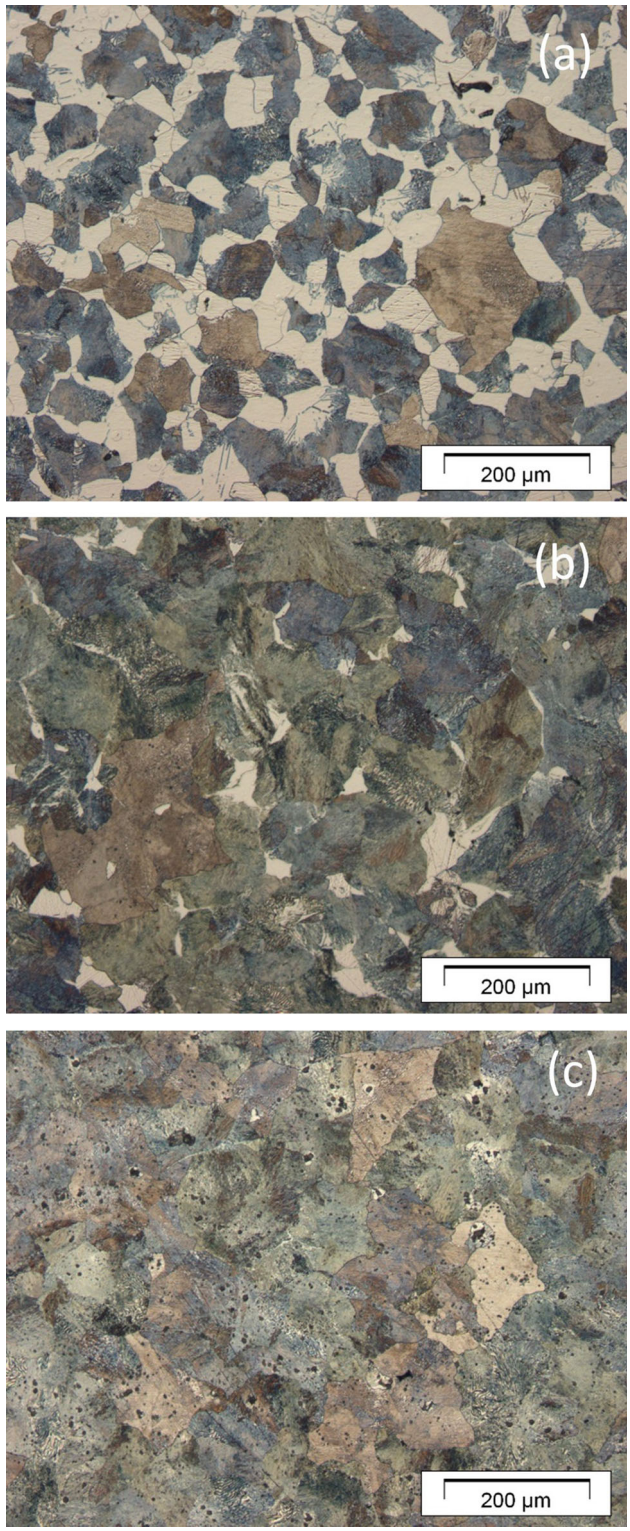

Fig. 1 LOM images of (a) A11, (b) A12, and (c) A13 in as-rolled conditions

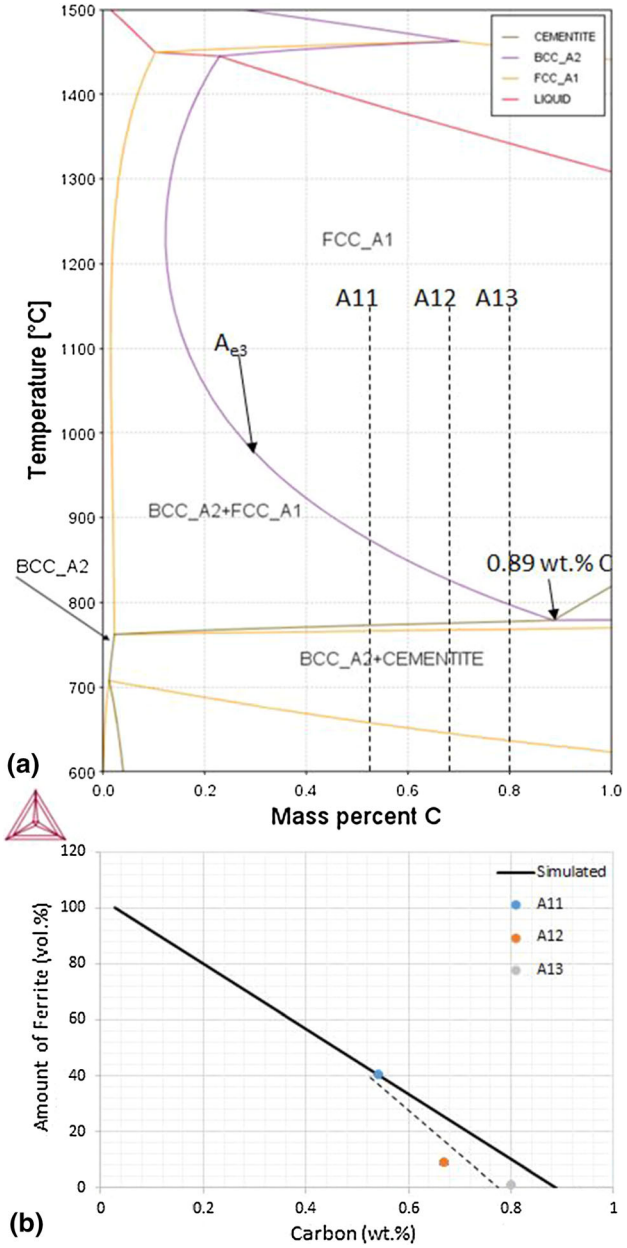

Fig. 2 (a) Phase diagram for the A1 alloy system calculated using ThermoCalc software and (b) comparison of the pro-eutectoid ferrite percentages obtained from the ThermoCalc simulation with the experimentally obtained values

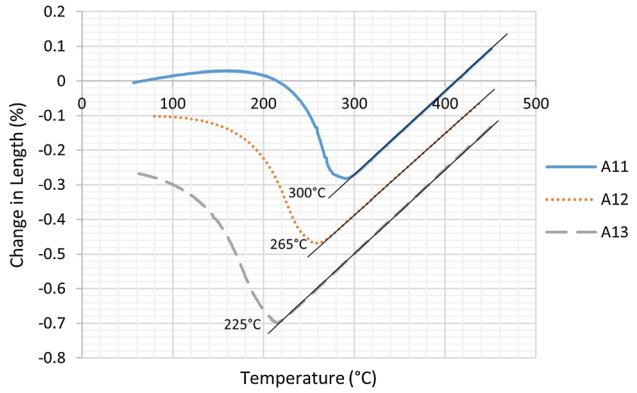

Fig. 3 Dilatation vs. temperature curves during quenching

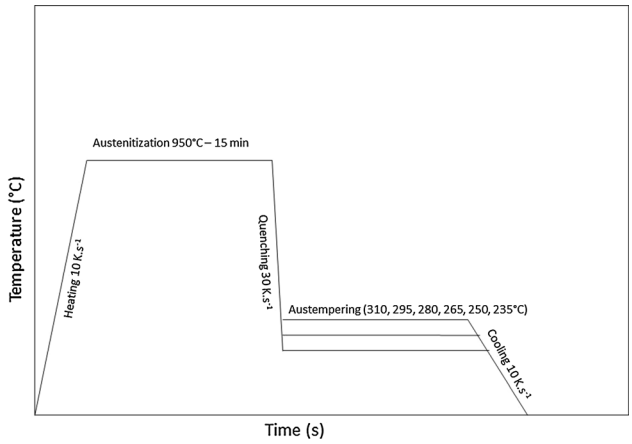

Fig. 4 Thermal cycles used to generate the different processing conditions tested

Table 2 Austempering temperatures used for each alloy

Alloy	Transformation temperature, °C					
A11						310
A12				280	295	310
A13	235	250	265	280	295	310

to 950 °C and held for 15 min, followed by quenching at a rate of 100 K s^{-1} to define the Ms temperature. Typical temperature versus change in length curves for the alloys introduced are shown in Fig. 3.

Ms temperatures for A11, A12, and A13 alloys were found to be 300, 265, and 225 °C, respectively. Figure 4 describes the thermal cycles used for bainitic transformation, with the different austempering temperatures for each alloy given in Table 2.

Figure 5 shows the dilatometric curves (a) and the variation of bainite transformation time with austempering holding temperatures for the three alloys studied (b). The usual trends can be observed with the transformation time increasing with C%, with the alloy A11 (0.539% C) requiring 650 s to finish its transformation at 310 °C, and A13 alloy (0.8% C) requiring 1700 s to reach the same conditions. The transformation time also increases with the reduction in the austempering temperature reaching up to 6800 s for A13 alloy at 235 °C. Recent publications in the field report minimum transformation times in the range of 4-7 h (Ref 9, 13, 31, 32); older studies report values up to several days (Ref 9-11, 33). The coupled effect of low Mn additions (0.29%) along with a moderately high Al percentage (0.9%) succeeded in significantly accelerating the bainitic transformation.

3.3 Mechanical Testing

Tensile strength and hardness results match the expected trends previously reported in the literature, as shown in Fig. 6(a), with strength increasing with decreasing austempering temperature and increasing C concentration (Ref 3, 32, 34,

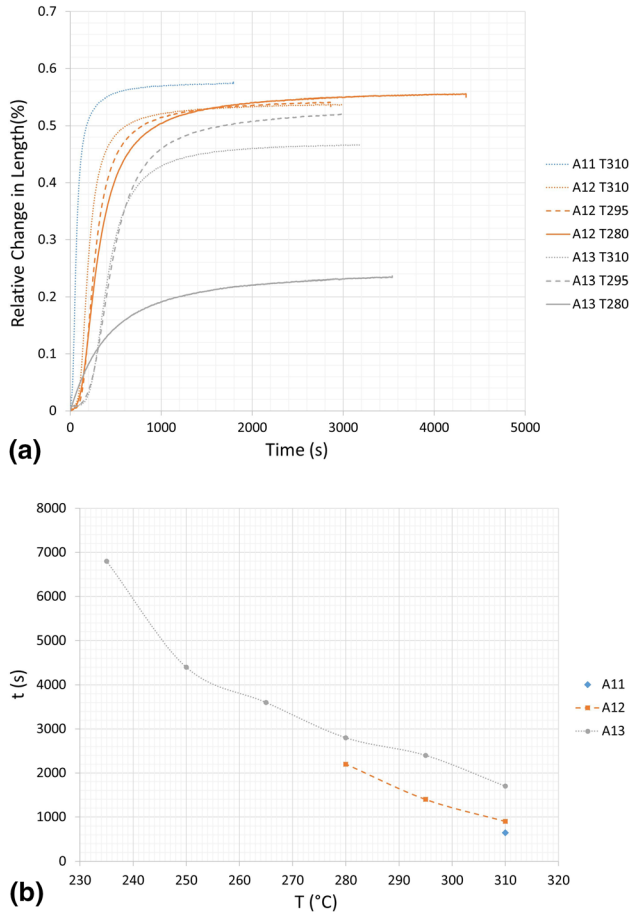

Fig. 5 (a) Dilation vs. time curves for the austempered alloys and (b) variation of bainitic transformation time with austempering temperature

35). Total elongation (EL%) and impact energy values (Fig. 6b and c), while low, still lie within the ranges reported in the literature for nB, namely 5-30 EL% and 5-35 J for the impact energy (Ref 3, 4, 7, 32, 35). Hardness values exceeding 600 HV have been recorded for all conditions, with a maximum of 720 HV for A13 alloy austempered at 235 °C. High tensile strength values (1900-2140 MPa) were reached for all alloys above an austempering temperature of 280 °C. However, no tensile testing data could be obtained for alloy A13 at austempering temperatures below 280 °C, as the notch sensitivity of the resulting microstructure significantly increased and the sub-size tensile specimens used constantly broke near the shoulders. nB structures are reported to be sensitive to notches and pre-cracks, which had been related by Belkin et al. to a high dislocation density and dislocation pileup, which is prevalent in nB structures (Ref 36, 37). This is, however, beyond the scope of this research project's objectives and experimental plan and thus was not investigated further in this publication.

3.4 XRD

Retained austenite values (Fig. 7b) obtained from Synchrotron XRD (Fig. 7a) show extremely low γ_r values, ranging from 14 to 3.5% (A11 alloy). While γ_r amounts as low as 10% have been previously reported (Ref 24), these values are overall much lower than the ranges common in the literature (20-30%) (Ref 3). Such results would imply either martensite formation or cementite precipitation. Martensite formation—if present—would be expected at the central regions of the blocky austenite, as a result of a lower C% and consequently lower austenite stability when compared to the regions closer to bainitic ferrite. SEM micrographs (Fig. 8) indicate the formation of some martensite upon cooling. The martensite seems to be formed only from larger blocky austenite regions, which seem to have not been sufficiently stabilized by carbon partitioning into them. This observation is congruent with the low retained austenite values obtained from the XRD testing.

The T_0 curve (Fig. 9) is the locus of all the points where austenite and ferrite of the same carbon content have the same energy. Hence, it indicates the amount of austenite enrichment attainable before the bainitic reaction becomes thermodynamically impossible. The position of the T_0 curve is affected by changing temperature and certain alloying additions. Changing the carbon content, however, does not affect the position of the T_0 curve, meaning that the three alloys studied would have the same T_0 curve (Ref 3, 4, 11, 38). Consequently, the bainite increases at the expense of the retained austenite according to Eq 1:

$$C_\gamma = \bar{C} + V_b \frac{(\bar{C} - s)}{(1 - V_b)} \quad \text{(Eq 1)}$$

where C_γ is the austenite carbon content, $\bar{C}$ is the alloy nominal carbon content, V_b is the volume fraction of bainite, and s is the ferrite carbon content, taken as 0.03 wt.% according to (Ref 39).

The decrease in the retained austenite with increasing alloy carbon content is previously shown in Fig. 7.

Retained austenite carbon content C_γ values obtained by the Synchrotron XRD analysis exceed those predicted by the T_0 curve. This has been explained by Bhadeshia and Edmonds as a result of the inhomogeneous distribution of carbon between the highly enriched film austenite and the less enriched blocky austenite variant (Ref 38). The presence of martensite in the microstructure indicates that at least a considerable amount of the—less stable—blocky austenite has transformed and, consequently, the XRD C_γ measurements are expected to be skewed toward the highly enriched film austenite. However, observing the behavior of A13 it is noted that by decreasing the transformation temperature, the trend predicted by the T_0 curve is being departed toward lower C_γ values as the temperature decreases. This can be explained by the increase in the volume fraction of bainite formed and the simultaneous strengthening of austenite from which it forms. Both factors result in increasing the dislocation density. Finally, the dependence of the redistribution of carbon between the solid solution and dislocations on the dislocation density, which is getting higher by decreasing the temperature, could be the reason for such deviation (Ref 18).

3.5 Strain Aging

Figure 10 shows the strain-aging response for the three alloys considered in this study. A significant yield strength increase of 213 MPa for alloy A11 and approximately 250 MPa for A12 and A13 could be stated for all alloys after strain aging for 20 min at 170 °C. The alloys tested display a small drop in ductility of around 1-2%EL. The stress–strain curves here are selected ones, while the values mentioned in the text are calculated based on the average of all specimens tested.

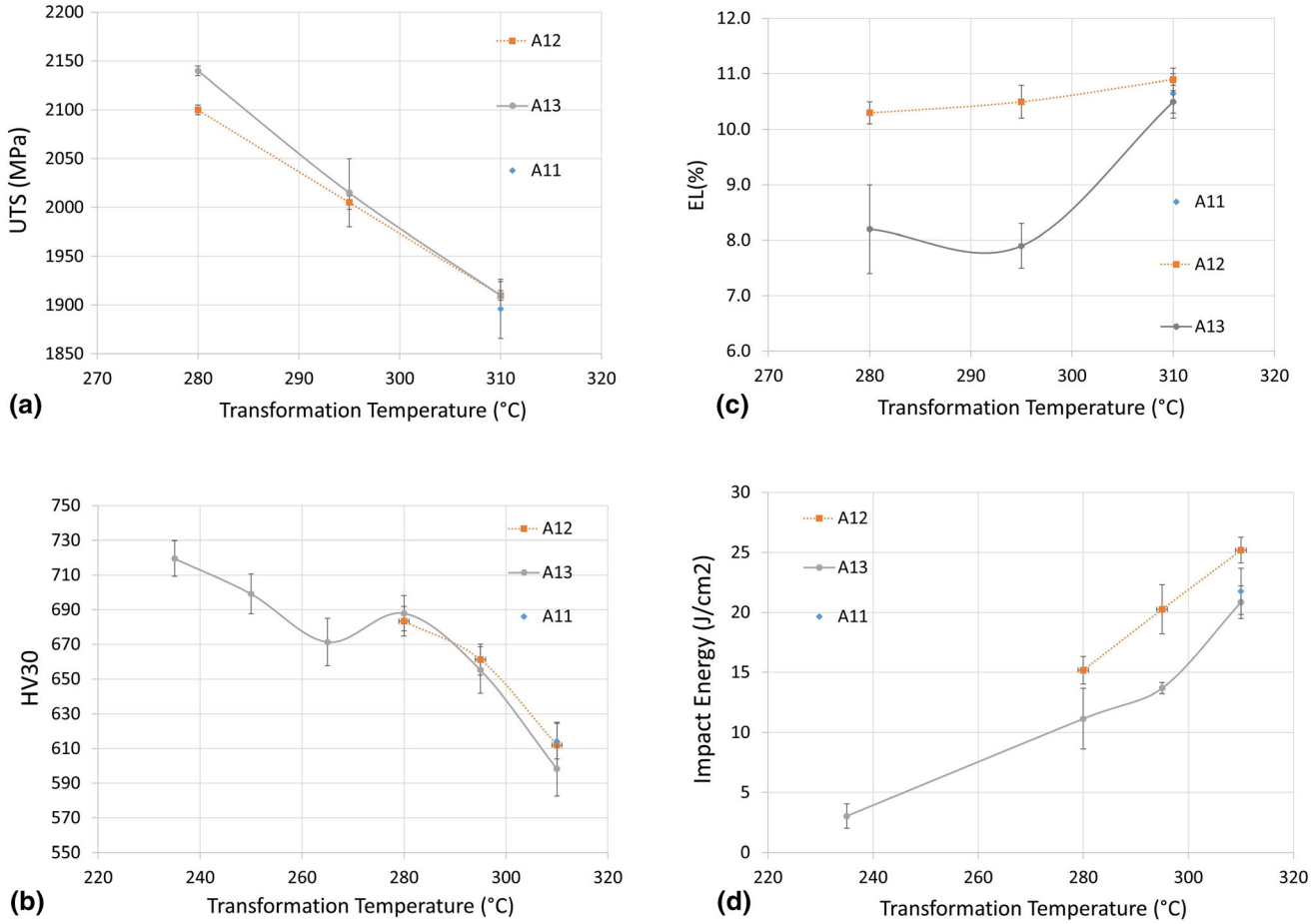

Fig. 6 Effect of changing austempering temperature on (a) ultimate tensile strength UTS, (b) hardness, (c) total elongation (EL%), and (d) impact energy

It is notable that the ductility drop of 1-2%EL corresponds to the amount of pre-straining the specimens were subjected to, implying that strain aging has no effect on the ductility of the aged alloy. A possible reason for the limited effect of strain aging on ductility could be that the main factor governing the ductility of the investigated alloys is expected to be the martensite, which would undergo at least partial tempering during the baking process. Hence, the final ductility would be affected by two opposing factors: strain aging reducing it and martensite tempering increasing it.

4. Discussion

While several other factors influence the bainitic reaction, it is mainly controlled by the driving force for ferrite formation. An increase in the free energy change—when austenite transforms to ferrite—would both accelerate the transformation kinetics, decrease the bainitic platelet thickness, as well as increase the amount of bainitic ferrite formed, consequently stabilizing more of the γ_r in the microstructure (Ref 40). Alloy A11 is a low-cost approach to maximize the aforementioned driving force. With relatively low C and Mn and moderate Al additions, the transformation time was in the order of 10 min (650 s). A high C content would serve to hinder the advancing ferrite-austenite interface, limiting the bainitic platelet thickness and consequently increasing strength. In addition to that, high C and Mn contents, which are austenite stabilizers, lower Ms. Thus, the drawbacks of this alloying strategy become clear, as both a high Ms and low C content would limit the maximum attainable strength value.

Reducing the Ms via C additions would slightly increase the transformation time (650 s for A11 to 1700 s for A13 at 310 °C), while the lowered Ms (225 °C for A13 versus 300 °C for A11) significantly increases the maximum attainable tensile strength (2140 MPa for A13 at 280 °C versus 1900 MPa for A11 at 310 °C). The literature reports the total elongation of nB steels to be in the range of 5-30% elongation. The lowest values of this range should, however, be due to the presence of martensite in the microstructure. The instability of blocky austenite has been discussed repeatedly in the literature. Blocky austenite is reported to transform to martensite at low loading, or even only upon cooling to room temperature (Ref 4, 9, 13, 41). SEM micrographs (Fig. 8) imply that the martensite originated from unstable blocky austenite. Another interesting observation is that the size of the austenite blocks that are decomposed into martensite is significantly larger than the austenite blocks that were stabilized. This is expected as the larger the austenite block is, the more difficult it is for C to diffuse into its centre and, hence, the less stable it becomes. In addition to that, the literature reports a close relationship between austenite grain size and suppression of martensite formation (Ref 42). The presence of low-stability austenite

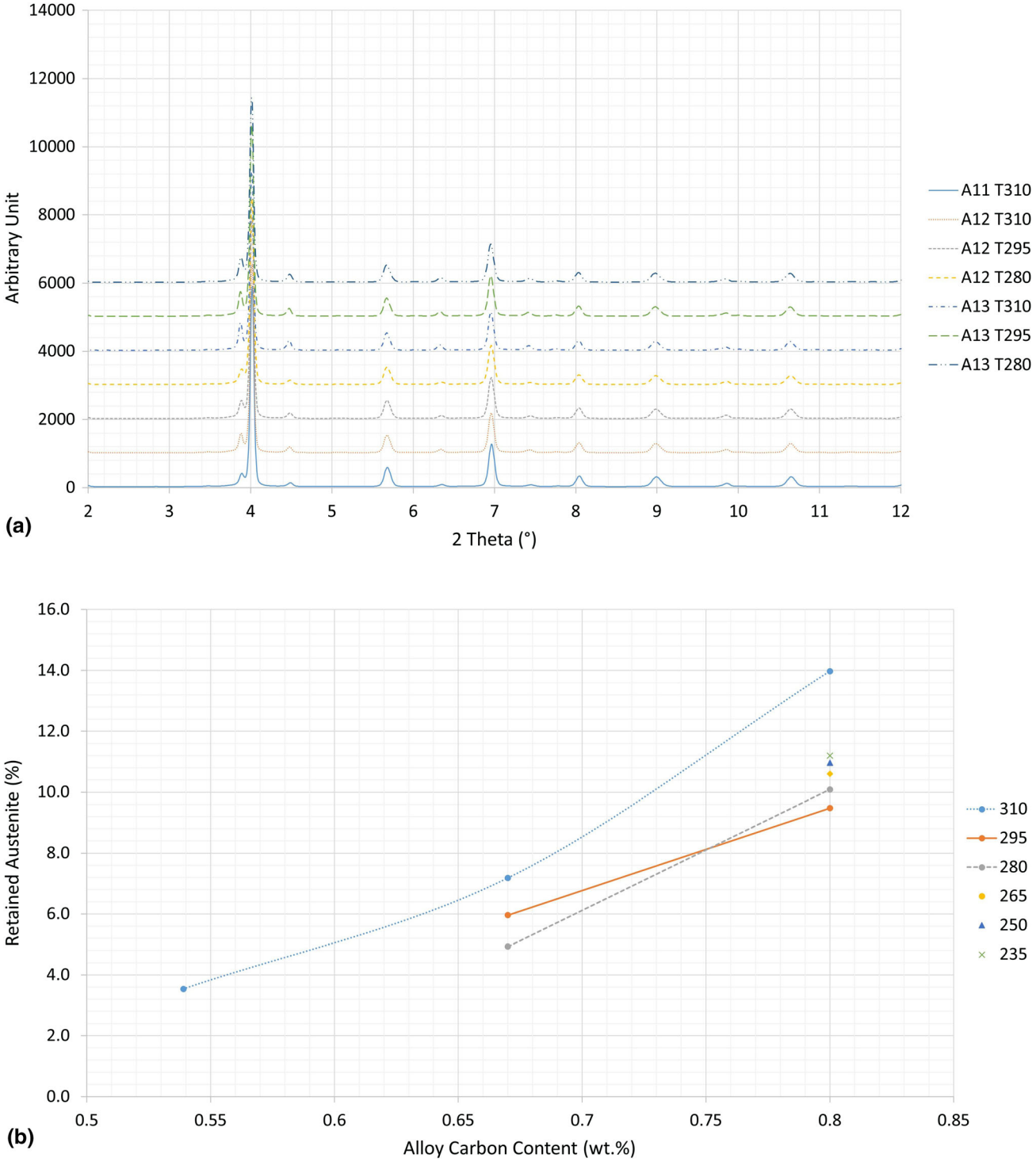

Fig. 7 (a) XRD patterns of the conditions tested and (b) variation of retained austenite with nominal carbon content

blocks in the microstructure could explain the low ductility values recorded for all the alloys studied (~ 10 EL%), since even if it were stable upon cooling to room temperature, these blocks would be expected to decompose into martensite at low loads during tensile testing, reducing the alloy's ductility.

Austenite stability is reported to depend on a number of factors, chemical stabilization via elements such as C and Mn, mechanical stabilization via increased dislocation density, and a reduction in austenite grain size (Ref 42). Alloying with low amounts of Mn and high amounts of Al, while beneficial in accelerating the transformation, was inadequate in stabilizing the larger-sized portions of the retained austenite population. The stability—or lack thereof—of the austenite present should be analyzed, in terms of the aforementioned factors, for each of the different retained austenite morphologies present in the microstructure. In the alloys investigated, several populations of retained austenite could be found (Fig. 8). The film austenite is both, chemically stabilized by carbon which partitioned into

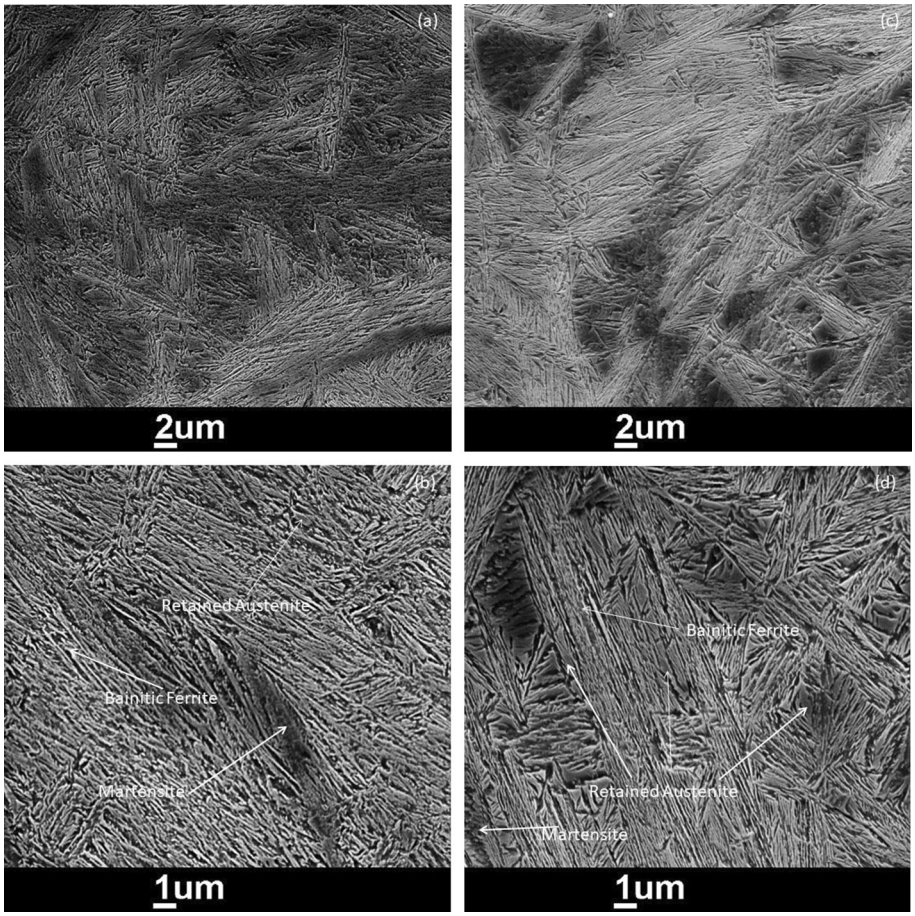

Fig. 8 SEM micrographs of (a, b) A11 alloy transformed at 310 °C and (c, d) A13 alloy transformed at 310 °C

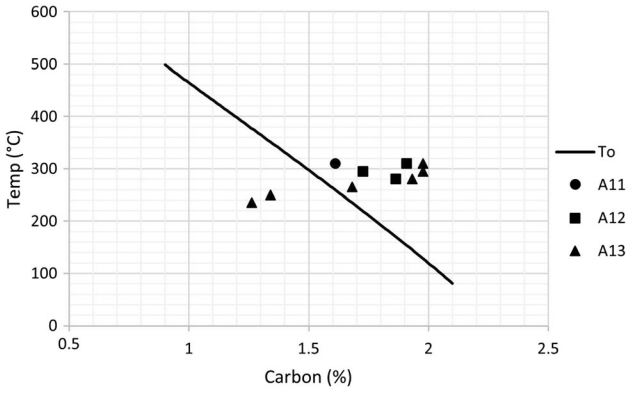

Fig. 9 T_0 curve of the alloy system studied

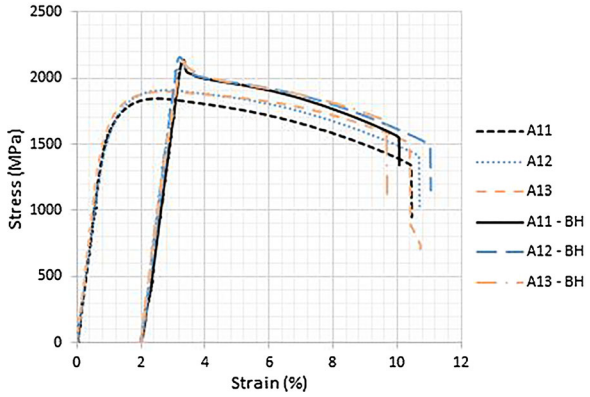

Fig. 10 Stress–strain curves of representative samples austempered at 310 °C together with those after 2% pre-straining and aging at 170 °C for 20 min

it during the bainitic transformation and mechanically by the hard bainitic ferrite platelets restricting its transformation. The blocky austenite, however, is not mechanically restricted by surrounding hard phases; hence, chemical stabilization and grain size are the only factors controlling its transformation into martensite. Due to the condition of para-equilibrium existing during the bainitic transformation, the blocky austenite is expected to inherit the substitutional element composition of the alloy at its austenitization temperature (here 0.29% Mn is relevant), while, on the other hand, its carbon content is dependent on the diffusion distance from the nearest transforming bainitic ferrite, which could be related to the austenite grain size. This implies a compound relationship between austenite grain size and its stability, where the grain size directly affects the transformation into martensite, as well as indirectly through influencing carbon diffusion and consequently chemical stability. This would explain why the smaller populations of retained austenite were stable after cooling while the larger populations transformed into martensite. Similar findings were reported by Lee et al. for TRIP steel where the

final alloy composition only stabilized austenite grains smaller than 500 nm (Ref 42).

5. Conclusions

Low-cost, high-strength, fast-transforming nB steel alloys were designed via the addition of Al and reduction in Mn content without relying on expensive alloying elements, mainly Co, as well as Cr and Ni in some cases. High tensile strength values ranging from 1900 to 2140 MPa were obtained at minimum transformation time of around 10 min for 0.54 wt.% C variant at 310 °C, and a maximum transformation time of less than 2 h was recorded for the 0.8 wt.% C variant at 235 °C. The recorded low ductility values of ~ 10 EL% are attributed to the instability of the larger-sized blocky austenite grains present in the microstructure and their transformation into martensite upon cooling to room temperature. The alloys studied displayed a significant strain-aging response with values of 213-250 MPa and minimal loss of ductility.

Acknowledgment

The authors are grateful to the Helmholtz-Zentrum Geesthacht (HZG) at the Deutsches Elektronen-Synchrotron (DESY) facility in Hamburg, Germany, and Dr. Eng. Emad Maawad for performing the synchrotron XRD measurements.

Funding

This work was supported by the Deutsche Forschungsgemeinschaft (DFG), Project Number SO 1250/1-1.

References

1. J. He, A. Zhao, Y. Huang, C. Zhi, and F. Zhao, Acceleration of Bainite Transformation at Low Temperature by Warm Rolling Process, *Mater. Today Proc.*, 2015, **2**, p S289–S294. https://doi.org/10.1016/j.matpr.2015.05.040
2. S.H. He, B.B. He, K.Y. Zhu, and M.X. Huang, On the Correlation Among Dislocation Density, Lath Thickness and Yield Stress of Bainite, *Acta Mater.*, 2017, **135**, p 382. https://doi.org/10.1016/j.actamat.2017.06.050
3. M. Soliman and H. Palkowski, Development of the Low Temperature Bainite, *Arch. Civ. Mech. Eng.*, 2016, **16**(3), p 03. https://doi.org/10.1016/j.acme.2016.02.007
4. M.N. Yoozbashi, S. Yazdani, and T.S. Wang, Design of a New Nanostructured, High-Si Bainitic Steel with Lower Cost Production, *Mater. Des.*, 2011, **32**(6), p 3248. https://doi.org/10.1016/j.matdes.2011.02.031
5. W. Gong, Y. Tomota, M.S. Koo, and Y. Adachi, Effect of Ausforming on Nanobainite Steel, *Scr. Mater.*, 2010, **63**(8), p 819. https://doi.org/10.1016/j.scriptamat.2010.06.024
6. W. Gong, Y. Tomota, S. Harjo, Y.H. Su, and K. Aizawa, Effect of Prior Martensite on Bainite Transformation in Nanobainite Steel, *Acta Mater.*, 2015, **85**, p 243. https://doi.org/10.1016/j.actamat.2014.11.029
7. A. Varshney, S. Sangal, S. Kundu, and K. Mondal, Super Strong and Highly Ductile Low Alloy Multiphase Steels Consisting of Bainite, Ferrite and Retained Austenite, *Mater. Des.*, 2016, **95**, p 75. https://doi.org/10.1016/j.matdes.2016.01.078
8. M. Soliman and H. Palkowski, Microstructure Development and Mechanical Properties of Medium Carbon Carbide-Free Bainite Steels, *Procedia Eng.*, 2014, **81**, p 1306. https://doi.org/10.1016/j.proeng.2014.10.148
9. M. Kabirmohammadi, B. Avishan, and S. Yazdani, Transformation Kinetics and Microstructural Features in Low-Temperature Bainite After Ausforming Process, *Mater. Chem. Phys.*, 2016, **184**, p 306. https://doi.org/10.1016/j.matchemphys.2016.09.057
10. F.G. Caballero and H.K.D.H. Bhadeshia, Very Strong Bainite, *Curr. Opin. Solid State Mater. Sci.*, 2004, **8**(3–4), p 251. https://doi.org/10.1016/j.cossms.2004.09.005
11. F.G. Caballero, H.K.D.H. Bhadeshia, K.J.A. Mawella, D.G. Jones, and P. Brown, Very Strong Low Temperature Bainite, *Mater. Sci. Technol.*, 2002, **18**(3), p 279. https://doi.org/10.1179/026708301225000725
12. H. Amel-Farzad, H.R. Faridi, F. Rajabpour, A. Abolhasani, S. Kazemi, and Y. Khaledzadeh, Developing Very Hard Nanostructured Bainitic Steel, *Mater. Sci. Eng. A*, 2013, **559**, p 68. https://doi.org/10.1016/j.msea.2012.08.020
13. S. Golchin, B. Avishan, and S. Yazdani, Effect of 10% Ausforming on Impact Toughness of Nano Bainite Austempered at 300 °C, *Mater. Sci. Eng. A*, 2016, **656**, p 94. https://doi.org/10.1016/j.msea.2016.01.025
14. J. Zhao, X. Jia, K. Guo, N.N. Jia, Y.F. Wang, Y.H. Wang, and T.S. Wang, Transformation Behavior and Microstructure Feature of Large Strain Ausformed Low-Temperature Bainite in a Medium C–Si Rich Alloy Steel, *Mater. Sci. Eng. A*, 2017, **682**, p 527. https://doi.org/10.1016/j.msea.2016.11.073
15. A. Eres-Castellanos, L. Morales-Rivas, A. Latz, F.G. Caballero, and C. Garcia-Mateo, Effect of Ausforming on the Anisotropy of Low Temperature Bainitic Transformation, *Mater. Charact.*, 2018, **145**, p 371. https://doi.org/10.1016/j.matchar.2018.08.062
16. H. Hu, G. Xu, F. Dai, J. Tian, and G. Chen, Critical Ausforming Temperature to Promote Isothermal Bainitic Transformation in Prior-Deformed Austenite, *Mater. Sci. Technol.*, 2019, **35**(4), p 420. https://doi.org/10.1080/02670836.2019.1567663
17. Y. Toji, H. Matsuda, and D. Raabe, Effect of Si on the Acceleration of Bainite Transformation by Pre-existing Martensite, *Acta Mater.*, 2016, **116**, p 250. https://doi.org/10.1016/j.actamat.2016.06.044
18. M. Soliman and H. Palkowski, Ultra-fine Bainite Structure in Hypo-Eutectoid Steels, *ISIJ Int.*, 2007, **47**(12), p 1703. https://doi.org/10.2355/isijinternational.47.1703
19. H. Palkowski, *Thermomechanisch hergestellter extrem fester Bainit mit reduziertem C-Gehalt*, Deutsche Forschungsgemeinschaft (DFG), 2011
20. C. Garcia-Mateo and F.G. Caballero, Ultra-high-strength Bainitic Steels, *ISIJ Int.*, 2005, **45**(11), p 1736. https://doi.org/10.2355/isijinternational.45.1736
21. S.M. Hasan, M. Ghosh, D. Chakrabarti, and S.B. Singh, Development of Continuously Cooled Low-Carbon, Low-Alloy, High Strength Carbide-Free Bainitic Rail Steels, *Mater. Sci. Eng. A*, 2020, **771**, p 138590. https://doi.org/10.1016/j.msea.2019.138590
22. H.-S. Yang and H.K.D.H. Bhadeshia, Designing Low Carbon, Low Temperature Bainite, *Mater. Sci. Technol.*, 2008, **24**(3), p 335. https://doi.org/10.1179/174328408x275982
23. J. Wang, P.J. van der Wolk, and S. van der Zwaag, On the Influence of Alloying Elements on the Bainite Reaction in Low Alloy Steels During Continuous Cooling, *J. Mater. Sci.*, 2000, **35**(17), p 4393. https://doi.org/10.1023/a:1004865209116

24. M. Soliman and H. Palkowski, *Verfahren zum Herstellen eines Bauteils mit bainitischem Gefüge und entsprechendes BauteilDE 102012017143B3 I*, 30 August 2012
25. J.-Y. Tian, G. Xu, M.-X. Zhou, H.-J. Hu, and Z.-L. Xue, Effects of Al Addition on Bainite Transformation and Properties of High-Strength Carbide-Free Bainitic Steels, *J. Iron Steel Res. Int.*, 2019, **17**(1), p 49. https://doi.org/10.1007/s42243-019-00253-7
26. E28 Committee, *Test Methods for Tension Testing of Metallic Materials*. ASTM International, West Conshohocken. https://doi.org/10.1520/e0008_e0008m-16a
27. DIN EN ISO 6892-1:2017-02, *Metallische Werkstoffe_- Zugversuch_- Teil_1: Prüfverfahren bei Raumtemperatur (ISO_6892-1:2016); Deutsche Fassung EN_ISO_6892-1:2016*. Beuth Verlag GmbH, Berlin. https://doi.org/10.31030/2384831
28. E28 Committee, *Test Methods for Notched Bar Impact Testing of Metallic Materials*. ASTM International, West Conshohocken. https://doi.org/10.1520/e0023-18
29. B.D. Cullity and S.R. Stock, *Elements of X-ray Diffraction*, 3rd ed., Prentice Hall, London, 2001
30. M. Soliman and H. Palkowski, Tensile Properties and Bake Hardening Response of Dual Phase Steels with Varied Martensite Volume Fraction, *Mater. Sci. Eng. A*, 2020, **777**, p 139044. https://doi.org/10.1016/j.msea.2020.139044
31. J. Yang, T.S. Wang, B. Zhang, and F.C. Zhang, Microstructure and Mechanical Properties of High-Carbon Si–Al-Rich Steel by Low-Temperature Austempering, *Mater. Des.*, 2012, **35**, p 170. https://doi.org/10.1016/j.matdes.2011.08.041
32. W. Liu, B. Zhang, A. Zhao, H. Guo, and S. Sun, Control of Morphology and Dimension of Blocky Retained Austenite in Medium-Carbon Steel, *Mater. Res. Express*, 2019, **6**(1), p 16526. https://doi.org/10.1088/2053-1591/aae561
33. H. Zou, H. Hu, G. Xu, Z. Xiong, and F. Dai, Combined Effects of Deformation and Undercooling on Isothermal Bainitic Transformation in an Fe–C–Mn–Si Alloy, *Metals*, 2019, **9**(2), p 138. https://doi.org/10.3390/met9020138
34. M. Soliman, H. Mostafa, A.S. El-Sabbagh, and H. Palkowski, Low Temperature Bainite in Steel with 0.26 wt% C, *Mater. Sci. Eng. A*, 2010, **527**(29–30), p 7706. https://doi.org/10.1016/j.msea.2010.08.037
35. J. Yang, H. Qiu, P. Xu, H. Yu, and Y. Wang, The Substitution of Aluminum for Cobalt in Nanostructured Bainitic Steels, *AIP Conf. Proc.*, 2018, **1971**(1), p 20001. https://doi.org/10.1063/1.5041096
36. A.M. Belkin, M.Y. Belkin, A.P. Vishnevskii, and V.I. Rulev, Notch Sensitivity of Structural Steels in Different Structural States, *Met. Sci. Heat Treat.*, 1989, **31**(1), p 42. https://doi.org/10.1007/bf00735328
37. F. Zhang and Z. Yang, Development of and Perspective on High-Performance Nanostructured Bainitic Bearing Steel, *Engineering*, 2019, **5**(2), p 319. https://doi.org/10.1016/j.eng.2018.11.024
38. H.K.D.H. Bhadeshia and D.V. Edmonds, Bainite in Silicon Steels: New Composition–Property Approach Part 2, *Met. Sci.*, 1983, **17**(9), p 420. https://doi.org/10.1179/030634583790420646
39. H.K.D.H. Bhadeshia and D.V. Edmonds, Bainite in Silicon Steels: New Composition–Property Approach Part 1, *Met. Sci.*, 1983, **17**(9), p 411. https://doi.org/10.1179/030634583790420600
40. C. Garcia-Mateo, F.G. Caballero, and H.K.D.H. Bhadeshia, Acceleration of Low-Temperature Bainite, *ISIJ Int.*, 2003, **43**(11), p 1821. https://doi.org/10.2355/isijinternational.43.1821
41. L. Guo, H. Roelofs, M.I. Lembke, and H.K.D.H. Bhadeshia, Modelling of Size Distribution of Blocky Retained Austenite in Si-Containing Bainitic Steels, *Mater. Sci. Technol.*, 2018, **34**(1), p 54. https://doi.org/10.1080/02670836.2017.1354797
42. S. Lee, S.-J. Lee, and B.C. de Cooman, Austenite Stability of Ultrafine-Grained Transformation-Induced Plasticity Steel with Mn Partitioning, *Scr. Mater.*, 2011, **65**(3), p 225. https://doi.org/10.1016/j.scriptamat.2011.04.010